DLL3 REGULATES NOTCH SIGNALING IN SCLC

Jun W. Kim[1,2#], Julie H. Ko[1,2#], and Julien Sage[1,2*]

Departments of [1]Pediatrics, [2]Genetics, Stanford University, Stanford, CA, USA.

[#]Equal contributions

*Correspondence to: Julien Sage, Stanford University, 265 Campus Drive, SIM1 G2078, Stanford, CA 94305-5457. Phone: 650-724-9246; Fax: 650-736-0195; E-mail: julsage@stanford.edu

ABSTRACT

Tumor heterogeneity plays a critical role in tumor development and response to treatment. In small-cell lung cancer (SCLC), intratumoral heterogeneity is driven in part by the Notch signaling pathway, which reprograms neuroendocrine cancer cells to a less/non-neuroendocrine state. Here we investigated the atypical Notch ligand DLL3 as a biomarker of the neuroendocrine state and a regulator of cell-cell interactions in SCLC. We first built a mathematical model to predict the impact of DLL3 expression on SCLC cell populations. We next tested this model using a single-chain variable fragment (scFv) to track DLL3 expression *in vivo* and a new mouse model of SCLC with inducible expression of DLL3 in SCLC tumors. We found that high levels of DLL3 promote the expansion of a SCLC cell population with lower expression levels of both neuroendocrine and non-neuroendocrine markers. This work may influence how DLL3-targeting therapies are used in SCLC patients.

INTRODUCTION

Intratumoral heterogeneity is a hallmark of cancer, with tumors consisting of a variety of cancer and non-cancer cells. This heterogeneity may vary over time and environmental conditions, including following therapy, and it can arise from genetic or epigenetic mechanisms. Intratumoral heterogeneity plays an important role in tumor development, including shaping the natural response of cancer cells to the immune system or treatment in the clinic (reviewed in (Black and McGranahan, 2021; Dagogo-Jack and Shaw, 2018; Jamal-Hanjani et al., 2015; Tammela and Sage, 2020)).

SCLC is an aggressive subtype of lung cancer with fast growth rates and a striking metastatic ability. The median overall survival of SCLC patients has remained close to 8-10 months in the past 3 decades, with a 5-year survival at ~6% and over 200,000 estimated deaths worldwide every year. Most tumors respond well initially to standard-of-care chemoradiation treatment, but resistance emerges rapidly in nearly all cases (reviewed in (Rudin et al., 2021)). The recent approval of T-cell immune checkpoint inhibitors has been beneficial to only a small fraction of SCLC patients (reviewed in (Barrows et al., 2022)). There is a critical need to develop biomarkers for SCLC development and more efficient therapeutic strategies.

Inter- and intratumoral heterogeneity are prominent in SCLC. SCLC tumors have been classified into different subtypes based on transcriptional programs driven by specific transcription factors, with the SCLC-A (expressing the ASCL1 transcription factor) and SCLC-N (expressing the NEUROD1 transcription factor) neuroendocrine subtypes being the most frequent in patients (Baine et al., 2020; Gay et al., 2021; Rudin et al., 2019). Importantly, mounting evidence indicates that individual SCLC tumors are comprised of heterogeneous populations of cancer cells with different levels of neuroendocrine gene programs (Calbo et al., 2011; Lim et al., 2017; Williamson et al., 2016). As an example of this intratumoral heterogeneity, in SCLC-A tumors, activation of Notch signaling can reprogram neuroendocrine (NE) cancer cells towards less/non-neuroendocrine (non-NE) phenotypes. The non-NE cells are less tumorigenic and genetic and pharmacologic approaches to promote NE to non-NE differentiation have been shown to decrease SCLC tumor growth (Augert et al., 2019). But non-NE can support the survival of the NE cells, including when tumors are treated with chemotherapy (Lim et al., 2017). In this context, the mechanisms activating Notch signaling are not completely understood, but may

depend on the YAP transcriptional regulator (Shue et al., 2022). As another example, in SCLC-N tumors, expression of c-MYC can activate Notch signaling, which also promotes the transition of these tumors to a less neuroendocrine phenotype (Ireland et al., 2020). These data and data from human tumors indicate that both inter- and intratumoral heterogeneity are likely key contributors of the ability of SCLC tumors to become resistant to therapies (Gay et al., 2021; Stewart et al., 2020; Sutherland et al., 2022).

DLL3 (Delta-like ligand 3) is an atypical ligand for NOTCH receptors initially studied for its role in early pattern formation in mouse embryos (Bulman et al., 2000; Dunwoodie et al., 1997; Kusumi et al., 1998). Early work showed that DLL3 is an inhibitor of Notch signaling in a cell autonomous manner (Ladi et al., 2005), possibly in a cis-inhibition mechanism in the Golgi (Chapman et al., 2011; Geffers et al., 2007). However, genetic studies of DLL3 O-fucosylation indicate that interactions with NOTCH may not fully account for the physiological function of DLL3, suggesting possible Notch-independent roles for DLL3 *in vivo* (Serth et al., 2015). The mouse *Dll3* gene is a direct target of ASCL1 (Nelson et al., 2009) and *DLL3* is expressed in a significant number of human SCLC tumors. Importantly, Saunders and colleagues showed that DLL3 is present at the surface of SCLC cells and that targeting DLL3-expressing SCLC cells using an antibody-drug conjugate (ADC) can eradicate SCLC in pre-clinical models (Saunders et al., 2015). Clinical trials using Rovalpituzumab tesirine (Rova-T), an ADC targeting DLL3, have been unsuccessful largely due to toxic side effects of this molecule (e.g., (Blackhall et al., 2021; Johnson et al., 2021; Malhotra et al., 2021)). However, other strategies are being developed to target DLL3 expressing cells, (e.g., (Giffin et al., 2021; Hipp et al., 2020; Lakes et al., 2020; Tully et al., 2022)) and DLL3 remains a target of interest for detection and treatment of SCLC.

Here we developed tools and models to further investigate the role of DLL3 as a biomarker of SCLC and as a regulator of Notch signaling in SCLC. We used mathematical modeling based on published data to predict the potential role that DLL3 expression may have on tumor heterogeneity. We further developed a new single-chain fragment variable (scFv) that can bind DLL3 on cells in culture and *in vivo.* Finally, we used this scFv to test our mathematical models in a new genetically engineered mouse model of SCLC with inducible expression of DLL3. Our data show variable levels of DLL3 expression in SCLC and indicate that DLL3 expression contributes to intratumoral heterogeneity.

RESULTS

Modeling the role of DLL3 in Notch-driven intratumoral heterogeneity in SCLC

DLL3 is often viewed as a cis-inhibitor of Notch signaling during development because of its role in localizing NOTCH receptors in the Golgi (**Figure 1A**). To determine if DLL3 could suppress Notch activity in SCLC cells, we used cells derived from tumors in the *Rb*$^{fl/fl}$*;p53*$^{fl/fl}$*;Rbl2*$^{fl/fl}$*;Hes1*$^{GFP/+}$ mouse model of SCLC (*RPR2;Hes1*^{GFP} model, also known as *TKO;Hes1*^{GFP}, for triple knockout) (Lim et al., 2017; Shue et al., 2022). In this model, SCLC cells express GFP when the *Hes1* promoter is active. Because *Hes1* is a target of Notch signaling, GFP expression can serve as a reporter of Notch activity, and HES1^{GFP}-positive (HES1^{pos}) cells are less/non-neuroendocrine (Lim et al., 2017; Shue et al., 2022). We isolated HES1^{pos} cells from *RPR2;Hes1*^{GFP} mutant tumors, and ectopic expression of FLAG-tagged DLL3 in these HES1^{pos} cells led to fewer GFP-positive cells, providing further evidence that DLL3 can suppress Notch signaling in *cis* in this SCLC context (**Figure 1B-D** and **Supplementary Figure S1A**).

In the Notch signaling pathway, activation of NOTCH receptors by their ligands, including Delta-like proteins (DLLs), leads to NOTCH cleavage, releasing the NOTCH intracellular domain (NICD). NICD induces transcription of the gene coding for HES1, which is an inhibitor of ASCL1, which is itself an activator of the expression of NOTCH ligands (DLLs, representing DLL1/3/4 and Jagged1/2 here) (Nelson et al., 2009; Ohsawa and Kageyama, 2008). This negative feedback leads to lateral inhibition and distinct cell fates among neighboring cells: low NOTCH/high DLL ('sender') cells and high Notch/low DLL ('receiver') cells (**Figure 1A**) (Collier et al., 1996). To gain a better understanding of the consequences of DLL3 expression on Notch signaling and intratumoral heterogeneity in SCLC, we built a simple mathematical model by incorporating DLL3 in the mutual inhibition model of lateral inhibition (Sprinzak et al., 2010) using the following reactions: (1) NOTCH receptors, denoted N, bind to DLL1 (as a representative of all NOTCH ligands, denoted D)in *trans*, which leads to cleavage of NOTCH and release of the Notch intracellular domain (NICD), denoted S; (2) NICD increases expression of HES1, denoted H (Bray 2006); (3) HES1 inhibits expression of DLL1 (Nelson et al., 2009; Ohsawa and Kageyama, 2008); (4) NOTCH receptors bind to DLL1 and DLL3, denoted D3, in *cis*, which inhibits NOTCH cleavage (Miller et al., 2009; Chapman et al., 2010; Ladi et al., 2005). As expected, setting the production rate of D3 at 0 replicated the results from

117 previous works on mutual inactivation (Sprinzak et al., 2010; Sprinzak et al., 2011)
118 supporting patterning even without cooperative regulatory feedback in the lateral
119 inhibition model (**Supplementary Figure S1B-G**). We simulated this model using 1600
120 parameter sets across a two-dimensional parameter space spanning a wide range of
121 production rates of D (β_D) and D3 (β_{D3}) (**Figure 1E**, **Equations 1-4** in Methods section,
122 and **Table S1** for parameter values). To represent multicellular interactions, a two-
123 dimensional hexagonal cell lattice was used for each parameter set. We plotted
124 $\log(H_{max}/H_{min})$, where H_{max} and H_{min} are the maximal and minimal HES1 levels in the
125 hexagonal lattice at the steady state, respectively, as a function of β_D and β_{D3} to observe
126 parameters leading to lateral inhibition, or heterogeneity in HES1 level (Formosa-Jordan
127 and Sprinzak 2014).

128 The cis-inhibition model shows that when $\beta_{D3} > \beta_D$, HES1 heterogeneity mostly does
129 not occur, indicating effective inhibition of cell-type bifurcation (**Figure 1E**). Within the
130 parameter regime leading to heterogeneity, β_{D3} also regulates the ratio of receiver
131 ($HES1^{high}$) cells and sender ($HES1^{low}$) cells, with higher number of sender cells as β_{D3}
132 increases (**Figure 1F**). We next examined H_{max} and H_{min} separately. H_{max} consistently
133 decreases as β_{D3} increases (**Figure 1G**). Interestingly, a large region of parameter space
134 shows higher H_{min} with increasing DLL3 (**Figure 1H,I**). H_{min} increases throughout the
135 parameter regime that leads to heterogeneity, peaking near $\beta_{D3} = \beta_D$, and gradually
136 decreases as β_{D3} further increases (**Figure 1H**).

137 In this system, our mathematical modeling suggests that the influence of DLL3 on the
138 heterogeneity of HES1 level depends on the level of DLL3 expression. At high levels (β_{D3}
139 $>> \beta_D$), DLL3 inhibits both heterogeneity and Notch activation. At lower levels, however,
140 DLL3 allows trans-interaction between NOTCH and other DLLs while preventing lateral
141 inhibition, which leads to homogeneous intermediate NOTCH activation throughout the
142 cell population. In the parameter space leading to heterogeneity, DLL3 expression also
143 affects sparsity of the receiver cells.

144 **Generation and validation of a single-chain fragment variable (scFv) binding DLL3**

145 Given that differences in DLL3 expression level may contribute to intratumoral
146 heterogeneity via NOTCH-driven patterning, we sought to examine whether DLL3 levels
147 in tumors were related to the amount of NOTCH signaling or intratumoral heterogeneity
148 present *in vivo*. To do this, we first developed a new tool to detect DLL3 in tumors *in vivo.*

149 Single-chain fragment variables (scFvs) have several advantages over antibodies,
150 including their small size and their ease of production in bacteria (Peltomaa et al., 2022;
151 Weisser and Hall, 2009). We generated a His-tagged scFv based on the sequence of an
152 antibody targeting DLL3 (Methods) (**Figure 2A and Supplementary Figure S2A**). We
153 first tested the binding of this scFv targeting DLL3 in 293T cells expressing exogenous
154 DLL3 compared to controls. Flow cytometry analysis using an anti-His antibody showed
155 increased binding in cells expressing mouse DLL3 (**Figure 2B,C**). Using the same
156 approach, we were also able to detect endogenous DLL3 expression in human SCLC cell
157 lines (**Figure 2C** and **Supplementary Figure S2B**). Thus, this scFv targeting DLL3 is
158 capable of binding to DLL3 expressed on the surface of SCLC cells in culture.

159 To determine if this scFv molecule (aDLL3scFv) could be useful to detect SCLC
160 tumors *in vivo*, we directly labeled the amino groups of lysine residues and the N-terminal
161 group of the aDLL3scFv with Alexa Fluor 680 (AF680), a near-infrared fluorophore with
162 strong tissue penetration that is suitable for *in vivo* imaging (**Figure 2D**). We first verified
163 that the AF680-labeled aDLL3scFv (aDLL3AF680) still detected DLL3 on the surface of
164 293T cells expressing exogenous DLL3 as well as SCLC cells in culture (**Figure 2E,F**
165 and **Supplementary Figure S2C**). Non-invasive optical imaging was performed over a
166 6-hour time period following tail-vein injections with 2 nmol of aDLL3AF680 in NSG mice
167 bearing subcutaneous xenografts (NCI-H82 model). Whole-body fluorescent imaging
168 showed prominent signal in the tumor area, as well as in the kidney (where the scFv
169 molecules are excreted) 2-3 hours post injection (**Figure 2G,H**). Maximum tumor-to-
170 normal tissue contrast was observed 2 hours post injection (**Supplementary Figure**
171 **S2D**). Signal from the fluorescent scFv was strong after 1 hour and started to decrease
172 after 3-4 hours, as expected for a small molecule with a short half-life (**Figure 2I**).

173 **Exogenous expression of DLL3 in mouse SCLC tumors**

174 Notch signaling is a driver of non-neuroendocrine cell fates and intratumoral
175 heterogeneity in SCLC (Ireland et al., 2020; Lim et al., 2017), and our mathematical
176 modeling predicts that DLL3 may contribute to Notch signaling activity and may modulate
177 heterogeneity. We next sought to test this idea experimentally in the *RPR2* mouse model
178 of SCLC where this heterogeneity has been described (Lim et al., 2017; Shue et al.,
179 2022). In this model, intra-tracheal instillation of an adenoviral vector expressing the Cre

180 recombinase initiates tumors modeling the SCLC-A subtype of human SCLC. SCLC cells
181 in these tumors express DLL3 at their surface (**Supplementary Figure S3A**).

182 To manipulate DLL3 levels in this model, we generated a new allele to conditionally
183 induce DLL3 expression upon Cre-mediated recombination (*Rosa26*$^{LSL\text{-}Dll3}$ allele) (**Figure**
184 **3A**). We crossed this allele to the *RPR2* model (*RPR2;Rosa26*$^{LSL\text{-}Dll3}$ mice) and initiated
185 tumors by Ad-CMV-Cre instillation. As controls, we used *RPR2;Rosa26*$^{LSL\text{-}Luc}$ mice
186 (Jahchan et al., 2016). Tumors developed in *RPR2;Rosa26*^{Dll3} mice, and their histology
187 was indistinguishable from that of *RPR2;Rosa26*^{Luc} mice; while we did not generate
188 enough mice to rigorously quantify tumor number and tumor burden, we did not observe
189 any striking difference in tumor development between the two models (**Figure 3B**). A cell
190 line derived from a *RPR2;Rosa26*^{Dll3} mutant lung tumor grew as spherical clusters in
191 suspension typical of neuroendocrine SCLC cell lines (Lim et al., 2017) and showed weak
192 but detectable expression of the tdTomato reporter linked to DLL3 expression, as well as
193 the expected recombination of the *Lox-STOP-Lox* cassette, validating the new allele
194 (**Figure 3A** and **Supplementary Figure S3B,C**).

195 We analyzed tumors from *RPR2;Rosa26*^{Dll3} and *RPR2;Rosa26*^{Luc} mutant mice ~5-6
196 months after tumor initiation for DLL3 expression using aDLL3scFv. In control
197 *RPR2;Rosa26*^{Luc} tumors, we observed two populations of cancer cells, as would be
198 expected for tumors with neuroendocrine (high DLL3) and less/non-neuroendocrine (low
199 DLL3) cells (**Figure 3C,D**). We validated this using NCAM and ICAM staining, with
200 NCAM^{high} ICAM^{low} cells representing neuroendocrine cells and NCAM^{low} ICAM^{high} cells
201 representing less/non-neuroendocrine, as validated previously by RNA-sequencing of
202 these two populations from *RPR2* tumors (Shue et al., 2022) (**Figure 3E,F**). In
203 *RPR2;Rosa26*^{Dll3} mutant tumors, we observed fewer cells with low levels of DLL3 and a
204 more homogeneous population of cells expressing intermediate/high levels of DLL3
205 (**Figure 3C,D**), indicating that the *Rosa26*^{Dll3} allele can elevate DLL3 expression on the
206 surface of DLL3^{low} cells but does not result in further overexpression on the surface of
207 DLL3^{high} cells (**Figure 3C,D**). Similarly, while NCAM^{high} ICAM^{low} cells express higher level
208 of DLL3 compared to NCAM^{low} ICAM^{high}, no significant difference was detected between
209 those of NCAM^{high} ICAM^{low} cells and cells from *RPR2;Rosa26*^{Dll3} mutant tumors (**Figure**
210 **E, F**).

211 We next quantified HES1 expression as a marker of intratumoral heterogeneity in
212 *RPR2;Rosa26*^{Dll3} and *RPR2;Rosa26*^{Luc} mutant tumors, with HES1^{high} cells being Notch-
213 active and less/non-neuroendocrine. As expected, we found regions with variable
214 numbers of HES1-positive cells (Lim et al., 2017; Shue et al., 2022) (**Supplementary**
215 **Figure S3D**). However, we did not detect any significant change in heterogeneity based
216 on this marker between the two groups (**Supplementary Figure S3E**). While these
217 experiments indicate that higher levels of DLL3 in tumors do not block the ability of SCLC
218 cells to undergo a transition to a NOTCH-driven HES1-positive state, we reasoned that
219 immunostaining may not be quantitative enough to identify more subtle changes.

220 We used flow cytometry to compare the expression of NCAM and ICAM in primary
221 lung tumors from *RPR2;Rosa26*^{Dll3} and *RPR2;Rosa26*^{Luc} mice (**Figure 3G**). Compared to
222 *RPR2;Rosa26*^{Luc} tumors, we found that *RPR2;Rosa26*^{Dll3} tumors exhibited a significant
223 decrease in the NCAM^{low} ICAM^{high} non-neuroendocrine population with no significant
224 change in the NCAM^{high} ICAM^{low} neuroendocrine population (**Figure 3G-I**). The change
225 in the NCAM^{low} ICAM^{high} population was reflected by an increase in NCAM^{low} ICAM^{low}
226 cells in *RPR2;Rosa26*^{Dll3} tumors (**Figure 3G,J**).

227 The relatively homogeneous population in *RPR2;Rosa26*^{Dll3} tumors suggests that
228 higher expression of DLL3 in SCLC cells can inhibit the cell-fate bifurcation process
229 mediated by the Notch signaling pathway. These observations support a model in which
230 DLL3 contributes to Notch signaling activity in SCLC and may serve as a Notch pathway
231 inhibitor in SCLC tumors *in vivo*.

Discussion

Here we investigated the role of the atypical NOTCH ligand DLL3 in a mouse model of SCLC. In our three-pronged approach, we combined mathematical modeling, a new scFv molecule, and a new allele to induce DLL3 expression in mouse cells. We found that DLL3 expression contributes to the generation of specific subpopulations of SCLC cells, supporting a role for DLL3 in Notch signaling and in the control of intratumoral heterogeneity in SCLC.

While cell autonomous sources for intratumoral heterogeneity arise from various stressors and defects that generate genetic instability, non-cell autonomous contributors often involve signaling pathways that play critical roles during normal development and can modify the transcriptome of cancer cells. In this regard, a canonical process involves spatiotemporal regulation of the Notch signaling pathway. The Notch pathway is a highly conserved signaling mechanism implicated in both normal development and the progression of various cancer types. In different tissues, Notch signaling provides a binary fate switch through a biochemical feedback mechanism known as lateral inhibition, which regulates differentiation into different cancer cell types from an initially homogenous field of cells (reviewed in (Chitnis, 1995; Sjöqvist and Andersson, 2019)). Thus, the Notch signaling pathway promotes cell fate “bifurcation” rather than a specific cell fate. This contribution of Notch-mediated lateral inhibition to intratumoral heterogeneity has been investigated extensively in multiple settings, including breast cancer (Bocci et al., 2019), glioblastoma (Lim et al., 2015), and bladder cancer (Torab et al., 2021). To examine a potential role of DLL3 in SCLC in the classical Notch circuit, we incorporated DLL3 in the lateral inhibition model with a mutual inactivation model. Our mathematical modeling predicts that DLL3 expression can affect Notch signaling in several ways. As expected, when the production rate of DLL3 exceeds that of DLL1 ($\beta_{D3} > \beta_D$) heterogeneity sharply decreases, indicating that DLL3 effectively reduces lateral inhibition (**Figure 1E**). Within the parameter regime of heterogeneity, DLL3 expression modulates the relative number of HES1^{pos} cells, making them sparser with increased DLL3 expression (**Figure 1F**). Interestingly, while very high production rates of DLL3 ($\beta_{D3} >> \beta_D$) lead to inhibition of Notch activation in the entire population, over a wide range of parameters DLL3 expression maintains an intermediate level of Notch activation, which peaks near $\beta_{D3} = \beta_D$ (**Figure 1H,I**). This observation reflects two seemingly opposing effects on Notch

signaling. Low levels of DLL3 are sufficient to inhibit lateral inhibition, reducing or preventing the rise of HES1^{low} cells. At very high levels, DLL3 inhibits Notch activation entirely through complete cis-inhibition. In between these two states, the trans-activation of Notch by DLL1 reinforces intermediate Notch activity, even within the parameter regime that leads to the homogenous state. Thus, in the context of SCLC, our theoretical framework predicts that while high levels of DLL3 promotes the HES1^{low} phenotype (neuroendocrine), at lower levels it can lead to a hybrid phenotype that is neither HES1^{low} nor HES1^{high}. When we examined the role of DLL3 experimentally in these processes, we found that ectopic expression of DLL3 in HES1^{pos} cells results in decreased HES1 expression, supportive of a cis-inhibitory function for DLL3. Intriguingly, induction of DLL3 in a mouse model of SCLC revealed that this ectopic expression decreases the relative number of cells in the non-neuroendocrine (NCAM^{low} ICAM^{high}) population and increases that of a NCAM^{low} ICAM^{low} population, without significantly altering the neuroendocrine (NCAM^{high} ICAM^{low}) population of cancer cells. This result suggests that DLL3 inhibits the bifurcation of SCLC cell fates. In future studies, it will be interesting to examine the exact nature of the NCAM^{low} ICAM^{low} population in *RPR2;Rosa26^{Dll3}* tumors, such as whether these cells represent a precursor cell similar to lung epithelial cells during early lung development before Notch signaling is activated or another population of non-NE cells that do not require Notch (Hong et al., 2022). Our new mouse allele for DLL3 expression may also be useful to investigate how DLL3 plays Notch-dependent and Notch-independent roles both in developmental processes and in cancer.

Because several therapeutic approaches currently in clinical development rely on the expression of DLL3 on SCLC cells, validating its expression before and during treatment could benefit patients with SCLC. Monitoring DLL3 levels in SCLC cells could be used to track overall progression of SCLC and, as our data suggest, heterogeneity between SCLC cell subpopulations. PET imaging of DLL3 has been evaluated clinically using DLL3 targeting antibodies with promising results (Sharma et al., 2017). However, slow normal tissue clearance and requirement of radioisotopes with long half-lives hamper clinical application of antibodies as noninvasive imaging agents (Wei et al., 2020). Here, we generated an anti-DLL3 scFv (~1/8th the size of an antibody) labeled with a fluorophore (aDLL3AF680) with tissue penetration, allowing noninvasive optical imaging. aDLL3AF680 successfully labeled SCLC tumors *in vivo* with good tumor-to-normal tissue contrast in a short time frame (2 hours post injection). Fast clearance may lead to a

297 superior imaging agent for clinical application. Small size may allow better tissue
298 penetration. Thus, scFv DLL3 binder may be a great alternative to full-length antibodies
299 for *in vivo* detection and targeting of DLL3 in SCLC and other tumor types expressing this
300 molecule on their surface.

Methods

Ethics statement

Mice were maintained according to practices prescribed by the National Institute of Health at Stanford's Research Animal Facility (APLAC protocol #13565) and by the Institutional Animal Care and Use Committee (IACUC) at Stanford. Additional accreditation of Stanford Research Animal Facility was provided by the Association for Assessment and Accreditation of Laboratory Animal Care.

Synthesis of anti-DLL3 scFv

Escherichia coli BL21 (DE3) cells were transformed with anti-DLL3 scFv (Raum et al., 2017) with c-terminal hexahistidine tag in pET vector by VectorBuilder. The transformed cells were grown overnight in LB agar plates with 100 µg/mL ampicillin. A single colony from each plate was inoculated in LB broth containing ampicillin and grown overnight. The primary culture was diluted 1:100 and grown at 37ºC. When OD_{600} reached 0.5, the cells were induced with IPTG 0.5 mM at 37ºC for 6 h. The cells were then harvested by centrifugation at 3,500 g, and the cell pellet was re-suspended with B-PER reagent (Thermo Fisher Scientific 90084) with lysozyme (0.1 mg/mL) and DNase I (50 µg/mL) and incubated for 30 min at 37ºC. Lysates were centrifuged at 15,000 × *g* for 10 min, and the supernatants were purified using a nickel-NTA affinity column (Qiagen 30210). Centrifugal filters with molecular 10 kDa molecular weight cutoffs (Millipore UFC801024) were used for further purification and buffer exchange into PBS. Protein purity was further analyzed using sodium dodecyl sulfate polyacrylamide gel electrophoresis and quantified using a plate reader.

AF680 dye conjugation

Purified scFv was buffer-exchanged to 0.1 M sodium bicarbonate buffer (pH 8.3) and concentrated to 3 mg/mL. AF680 succinimidyl ester (Thermo Fisher Scientific A20008) was dissolved in DMSO at 10 mg/mL and added to the protein solution to give a final concentration of 1 mg/mL. The reaction was incubated for 1 hr at room temperature. Unreacted dye removal and buffer exchange to PBS was done using a 10 kDa centrifugal filter.

Cell binding assays

$5x10^5$ human and mouse cells were incubated with 50 µL of 30 µg/mL aDLL3AF680

332 for 1 hr in PBS with 0.1% BSA (PBSB) at 4ºC. The cells were then washed twice with
333 PBSB and analyzed by flow cytometry. For testing unlabeled aDll3scFv, cells were
334 incubated with 50 µL of 30 µg/mL aDll3scFv for 1 hr in PBSB at 4ºC. The cells were
335 washed once with PBSB, and secondary binding was performed on ice for 30 min
336 using rabbit anti-hexahistidine antibody (Cell Signaling Technology 12698S) diluted
337 1:100 in PBSB. The cells were washed once with PBSB and incubated with goat anti-
338 rabbit antibody labeled with Alexa Fluor 488 (Invitrogen A11008) diluted 1:100 in
339 PBSB for 30 min on ice. The cells were then washed twice with PBSB before being
340 analyzed by flow cytometry.

341 **Cell culture**

342 Cell lines were cultured in RPMI-1640 (Corning MT15040CV) except for 293T cells
343 and cell lines derived from *RPR2;R26*^{Luc} and *RPR2;R26*^{Dll3}, which were cultured in
344 DMEM (Hyclone SH30243.01). RPMI and DMEM were supplemented with 10%
345 bovine growth serum (Hyclone SH3054103HI) and penicillin-streptomycin-glutamine
346 (Gibco 10378016). Cells were grown at 37ºC in standard cell culture incubators. All
347 cells were routinely tested (MycoAlert Detection Kit, Lonza) and confirmed to be free
348 of mycoplasma contamination.

349 NCI-H524, NCI-H82, and NCI-H1694 cells were purchased from ATCC. Murine
350 KP11B6 (a negative control for tdTomato expression in **Supplementary Figure S3B**)
351 and HES1$^{GFP/+}$ SCLC cell lines were generated in the lab and have been described
352 (Lim et al., 2017).

353 **Lentiviral transduction**

354 5x10^5 293T cells were seeded in each well of a 6-well plate and left to adhere
355 overnight in antibiotics-free DMEM High-Glucose medium supplemented with 10%
356 bovine growth serum. Lentiviral vectors were co-transfected with delta8.2 and VSV-G
357 lentiviral packaging vectors using PEI. The supernatant was collected after 48 hr and
358 added to the target cells. Cells were treated on day 5 with the selection agent
359 according to the lentiviral vector used.

360 **Plasmids/sequences**

361 For mammalian expression of DLL3, mouse DLL3 with a C-terminal FLAG-tag was
362 cloned into the pCDH lentiviral expression vector.

363 **Flow cytometry**

364 Flow cytometry was performed using a 100 μm nozzle on BD FACSAria II (Stanford
365 Stem Cell Institute FACS Core) and analyzed with the FACSDiva software. For single cell
366 analysis of lung tumors, a sequential gating strategy was used to analyze cancer cells by
367 staining with the following FACS antibodies (**Figure S3F**): CD45-Pacific Blue (BioLegend
368 103126, 1:100), CD31-Pacific Blue (BioLegend 102422, 1:100), TER-119-Pacific Blue
369 (BioLegend 116232, 1:100), CD24-APC (eBioscience 17-0242-82, 1:200), ICAM1-PE-
370 CY7 (BioLegend 116122, 1:100), and NCAM-PE (R&D Systems FAB7820P, 1:100)
371 (Shue et al., 2022). Data were analyzed using Flowjo software.

372 **Lateral inhibition with mutual inactivation (LIMI) model with DLL3**

373 Notch receptor (N_i) in cell *i* interacts with DLL1 (D_j) on the surface of a neighboring cell
374 *j*. This *trans*-activation leads to cleavage of the Notch receptor, which frees the
375 intracellular domain, NICD (S_i) to induce expression of downstream genes such as Hes1
376 (H_i), described by the class lateral inhibition model (Collier et al., 1996). Notch receptor
377 (N_i) also interact with DLL1 (D_i) on the same cell surface, which leads to cis-inhibition,
378 described by the LIMI model (Sprinzak et al., 2010). In order to see the effect of cis-
379 inhibition by DLL3 ($D3_i$), Notch receptor (N_i), and DLL1 (D_i) on the same cell surface, we
380 modified LIMI by considering the following system in two-dimensional array:

381 $N_i + D_j \rightleftharpoons [N_iD_j] \rightarrow S_i$ trans-activation
382 $S_i \rightarrow H_i$ Induction of Hes1 expression by Notch cleavage
383 $H_i \dashv D_i$ Repression of DLL1

384 $N_i + D_i \rightleftharpoons [N_iD_i] \rightarrow \emptyset$ cis-inhibition between Notch and DLL1
385 $N_i + D3_i \rightleftharpoons [N_iD3_i] \rightarrow \emptyset$ cis-inhibition between DLL3 and Notch

386 The first four reactions that do not describe DLL3 are directly from LIMI (Sprinzak et
387 al., 2010). This model can be described by the following set of equations applied to a two-
388 dimensional hexagonal lattice of cells:

$$\dot{N}_i = \beta_N - \gamma_N N_i - \frac{N_i D_j}{k_t} - \frac{N_i D_i}{k_c} - \frac{N_i D3_i}{k_e} \quad (1)$$

$$\dot{D}_i = \beta_D \frac{k_{DH}}{k_{DH} + H_i{}^m} - \gamma_D D_i - \frac{N_j D_i}{k_t} - \frac{N_i D_i}{k_c} \quad (2)$$

$$\dot{H}_i = \beta_H \frac{\left(\frac{N_i D_j}{k_t \gamma_s}\right)^p}{k_{HS} + \left(\frac{N_i D_j}{k_t \gamma_s}\right)^p} - \gamma_H H_i \quad (3)$$

$$\dot{D3}_i = \beta_{D3} - \gamma_{D3} D3_i - \frac{N_i D3_i}{k_e} \quad (4)$$

Equations 1-3 are from LIMI (Sprinzak et al., 2011). N_i and D_j interact at a rate k_t^{-1}. N_i and D_i interact at a rate k_c^{-1}. N_i, D_i, and H_i are produced at a rate of β_N, β_D, and β_H, respectively. N_i, D_i, and H_i are degraded at a rate of γ_N, γ_D, and γ_H, respectively. Repression of D_i by H_i is represented with a decreasing Hill function as a function of k_{DH} and m. Expression of H_i by S_i is represented with an increasing Hill function as a function of k_{HS} and p. Equation 4 describes $D3_i$, where $D3_i$ is produced, degraded, and interact with N_i at a rate β_{D3}, γ_{D3}, and k_e, respectively. These equations are used in Figure 1 and Supplementary Figure 1. For Supplementary Figure S1B, D, and F, the mutual inactivation represented by $\frac{N_i D_i}{k_c}$ was omitted.

Numerical computations were performed using MATLAB's ode15s solver (R2017b, MathWorks) using the scripts provided by Formosa-Jordan and Sprinzak (Formosa-Jordan and Sprinzak, 2014). The modified MATLAB codes can be downloaded from https://github.com/junwkim1/DLL3_lateral_inhibition_2022.

Mouse models

The *Rb1*$^{flox/flox}$*;Trp53*$^{flox/flox}$*;Rbl2*$^{flox/flox}$ *(RPR2,* or *TKO)* mouse model and the *Rosa26*$^{lox\text{-}stop\text{-}lox\text{-}luciferase}$ *(R26*^{Luc}*)* allele have been previously described (Jahchan et al., 2016; Schaffer et al., 2010). Mice were maintained in a mixed C57BL/6;129SVJ background.

Cre-inducible DLL3-overexpressing mice (*R26*^{Dll3}) were generated by knocking in a *Lox-Stop-Lox-Dll3-IRES-tdTomato* cassette into the *Rosa26* allele. The mice were generated by genOway via homologous recombination into the *Rosa26* allele in mouse embryonic stem cells, and clones were then injected into blastocysts to generate chimeric mice with germline transmission. The *Dll3* sequence in this allele is a cDNA/gDNA combo that retains intron 6 within the cDNA sequence to allow for

423 expression of potential splice variants.

424 *R26*$^{LSL\text{-}Dll3}$ mice were crossed to *RPR2;R26*$^{LSL\text{-}Luc}$ mice to generate *RPR2;R26*$^{LSL\text{-}Dll3/LSL\text{-}Luc}$
425 mice, which were then crossed to each other to generate *RPR2;R26*$^{LSL\text{-}Dll3/\ LSL\text{-}Dll3}$
426 mice and *RPR2;R26*$^{LSL\text{-}Luc/LSL\text{-}Luc}$ littermate controls. Tumors were initiated at 8-12
427 weeks of age with intratracheal instillation of $4x10^7$ plaque-forming units of Adeno-CMV-
428 Cre (Baylor College of Medicine, Houston, TX). Animals were euthanized and tumors
429 were collected at ~6.5 months post-initiation, or earlier if they showed signs of respiratory
430 distress. Mice were housed at 22°C ambient temperature with 40% humidity and a
431 light/dark cycle of 12 hours (7am – 7pm).

432 **Genotyping**

433 Mice were genotyped by using the Mouse Direct PCR kit (Bimake) on DNA isolated
434 from tails following the manufacturer's protocol.

	Forward	Reverse
Rb1^{flox}	5'-CCTTGACCATAGCCCAGCAC-3'	5'-CTCTAGATCCTCTCATTCTTCCC-3'
p53^{flox}	5'-GAAGACAGAAAAGGGGAGGG-3'	5'-AAGGGGTATGAGGGACAAGG-3'
Rbl2^{flox}	5'-GACTGCTGGTATTAGAACCC-3'	5'-GTGTTGTAACATTCTCGTGGG-3'
R26^{Luc}	5'-AAAGTCGCTCTGAGTTGTTAT-3'	5'-GCGAAGAGTTTGTCCTCAACC-3'
R26$^{LSL\text{-}Dll3}$	5'-AAGAAAAGCCAGGATCAGCGTCTGG-3'	5'-CACTGCATTCTAGTTGTGGTTTGTCCAAAC-3'
R26^{Dll3}	5'-AAGAAAAGCCAGGATCAGCGTCTGG-3'	5'-GGGCAACGTGCTGGTTATTG-3'
tdTomato	5'-TGGAGTGGCAACTTCCAGGG-3'	5'-ACGGCATGGACGAGCTGTA-3'

435 **Immunostaining**

436 Lung lobes were fixed overnight in 10% formalin in PBS before paraffin embedding.
437 Paraffin sections were deparaffinized with Histo-Clear (National Diagnostics HS-200) and
438 gradually rehydrated from ethanol to water. Antigen retrieval was carried out in citrate-
439 based unmasking solution (Vector Laboratories H-3300) by microwaving at full power until
440 boiling, then 30% power for 25 min (DLL3) or 15 min (HES1), then left to cool at room
441 temperature for 10 min before washing with water. Endogenous peroxidase was blocked
442 by incubating slides in 3% hydrogen peroxide for 1 h. Sections were washed in PBST
443 (PBS with 0.1% Tween-20), blocked in 5% horse serum for 1 h, and incubated with anti-

444 DLL3 (1:200 Invitrogen PA5-23448) or anti-HES1 (1:200 Cell Signaling Technology
445 11988) diluted in PBST overnight at 4°C. DLL3 was developed using
446 ImmPRESS®HRP Horse Anti-Rabbit IgG Polymer Detection Kit (Vector Laboratories
447 MP-7401) following the manufacturer's protocol. HES1 was developed using
448 ImmPRESS® Excel Amplified Polymer Staining Anti-Rabbit IgG Peroxidase Kit
449 (Vector Laboratories MP-7601) following the manufacturer's protocol. All sections
450 used DAB substrate kit (Vector Laboratories SK-4100) for color development.
451 Sections were counterstained with hematoxylin (Sigma-Aldrich HHS32-1L), gradually
452 dehydrated from water to ethanol to xylene, and mounted with Refrax mounting
453 medium (Anatech Ltd711). Sections were imaged using Keyence BZ-X700 all-in-one
454 fluorescence microscope with BZ-X Viewer program version 1.3.1.1 and BZ-X
455 Analyzer 1.4.0.1.

456 **Single-cell suspension**

457 Tumors were dissected from lungs between 5 to 6.5 months after tumor induction,
458 finely chopped with a razor blade, and digested for 15 min at 37°C in 10 mL of L-15
459 medium (Sigma L1518) containing 4.25 mg/mL Collagenase I (Sigma C0130), 1.4
460 mg/mL Collagenase II (Sigma 6885), 4.25 mg/mL Collagenase IV (Sigma 5138), 0.625
461 mg/mL Elastase (Worthington LS002292), and 0.625 mg/mL DNase I (Roche
462 10104159). The digested mixture was filtered through a 40 μm filter and centrifuged
463 at 400 g for 5 min at room temp, and the resulting pellet was resuspended in 1 mL
464 RBC lysis buffer (eBioscience 00-4333-57) for 30 sec, diluted in 30 mL PBS, and
465 centrifuged at 400 g for 5 min at room temp. The pelleted cells were then resuspended
466 in 0.1% BSA/PBS for flow cytometry or in cell culture media to generate cell lines.

467 **Statistical analysis**

468 Statistical significance was assayed with GraphPad Prism software. Data are
469 represented as mean ± sd. *$p<0.05$, **$p<0.01$, ***$p<0.001$, ****$p<0.0001$, ns not
470 significant. The tests used are indicated in the figure legend.

471 **Data availability**

472 All data are available in the article or from the corresponding author upon request.

Acknowledgements

The authors thank Dr. Laura Saunders and Dr. Chen-Hua Chuang at Abbvie/StemCentrx for their help during the course of this study, including with the generation of the *R26*$^{LSL\text{-}Dll3}$ mice. We would like to thank David S. Glass for discussions and advice, as well as Myung Chang Lee for his comments on the manuscript. We also thank Pauline Chu from the Stanford Histology Service Center and all the members of the Sage lab for their help throughout this study. Research reported in this publication was supported by the Ludwig Institute for Cancer Research (J.S.), the NIH (grants CA217450, CA213273, and CA231997 to J.S., CA257169 to J.H.K.), and the A.P. Giannini Foundation (J.W.K.).

Contributions

J.W.K., J.H.K, and J.S. designed the experiments, interpreted the results, and wrote the manuscript; J.W.K. performed the mathematical modeling and developed the scFv molecules; J.H.K performed experiments with mice; J.W.K. and J.H.K. worked together on experiments with cells in culture and tumor analysis.

Competing interests

J.S. received research funding from StemCentrx/Abbvie for the development of the new *Dll3* allele. J.S. has equity in, and is an advisor for, DISCO Pharmaceuticals. The authors declare no other competing interests.

References

Augert A., Eastwood E., Ibrahim A.H., Wu N., Grunblatt E., Basom R., Liggitt D., Eaton K.D., Martins R., Poirier J.T., Rudin C.M., Milletti F., Cheng W.Y., Mack F., MacPherson D., 2019. Targeting NOTCH activation in small cell lung cancer through LSD1 inhibition. Sci Signal 5, 12(567), eaau2922. https://doi.org/10.1126/scisignal.aau2922.

Baine, M.K., Hsieh, M.-S.S., Lai, W.V., Egger, J.V., Jungbluth, A.A., Daneshbod, Y., Beras, A., Spencer, R., Lopardo, J., Bodd, F., Montecalvo, J., Sauter, J.L., Chang, J.C., Buonocore, D.J., Travis, W.D., Sen, T., Poirier, J.T., Rudin, C.M., Rekhtman, N., Victoria Lai, W., Egger, J.V., Jungbluth, A.A., Daneshbod, Y., Beras, A., Spencer, R., Lopardo, J., Bodd, F., Montecalvo, J., Sauter, J.L., Chang, J.C., Buonocore, D.J., Travis, W.D., Sen, T., Poirier, J.T., Rudin, C.M., Rekhtman, N., Lai, W.V., Egger, J.V., Jungbluth, A.A., Daneshbod, Y., Beras, A., Spencer, R., Lopardo, J., Bodd, F., Montecalvo, J., Sauter, J.L., Chang, J.C., Buonocore, D.J., Travis, W.D., Sen, T., Poirier, J.T., Rudin, C.M., Rekhtman, N., 2020. SCLC Subtypes Defined by ASCL1, NEUROD1, POU2F3, and YAP1: A Comprehensive Immunohistochemical and Histopathologic Characterization. Journal of Thoracic Oncology 15, 1823–1835. https://doi.org/10.1016/j.jtho.2020.09.009

Barrows, E.D., Blackburn, M.J., Liu, S.V., 2022. Evolving role of immunotherapy in small cell lung cancer. Semin Cancer Biol S1044-579X(22)00048–7. https://doi.org/10.1016/j.semcancer.2022.02.021

Black, J.R.M., McGranahan, N., 2021. Genetic and non-genetic clonal diversity in cancer evolution. Nat Rev Cancer 21, 379–392. https://doi.org/10.1038/s41568-021-00336-2

Blackhall, F., Jao, K., Greillier, L., Cho, B.C., Penkov, K., Reguart, N., Majem, M., Nackaerts, K., Syrigos, K., Hansen, K., Schuette, W., Cetnar, J., Cappuzzo, F., Okamoto, I., Erman, M., Langer, S.W., Kato, T., Groen, H., Sun, Z., Luo, Y., Tanwani, P., Caffrey, L., Komarnitsky, P., Reinmuth, N., 2021. Efficacy and Safety of Rovalpituzumab Tesirine Compared With Topotecan as Second-Line Therapy in DLL3-High SCLC: Results From the Phase 3 TAHOE Study. Journal of Thoracic Oncology 16, 1547–1558. https://doi.org/10.1016/j.jtho.2021.02.009

Bocci, F., Gearhart-Serna, L., Boareto, M., Ribeiro, M., Ben-Jacob, E., Devi, G.R., Levine, H., Onuchic, J.N., Jolly, M.K., 2019. Toward understanding cancer stem cell heterogeneity in the tumor microenvironment. Proc Natl Acad Sci U S A 116, 148–157. https://doi.org/10.1073/pnas.1815345116

Bulman, M.P., Kusumi, K., Frayling, T.M., McKeown, C., Garrett, C., Lander, E.S., Krumlauf, R., Hattersley, A.T., Ellard, S., Turnpenny, P.D., 2000. Mutations in the human delta homologue, DLL3, cause axial skeletal defects in spondylocostal dysostosis. Nat Genet 24, 438–441. https://doi.org/10.1038/74307

Calbo, J., van Montfort, E., Proost, N., van Drunen, E., Beverloo, H.B., Meuwissen, R., Berns, A., 2011. A functional role for tumor cell heterogeneity in a mouse model of small cell lung cancer. Cancer Cell 19, 244–256. https://doi.org/10.1016/j.ccr.2010.12.021

Chapman, G., Sparrow, D.B., Kremmer, E., Dunwoodie, S.L., 2011. Notch inhibition by the ligand DELTA-LIKE 3 defines the mechanism of abnormal vertebral

537 segmentation in spondylocostal dysostosis. Hum Mol Genet 20, 905–916.
538 https://doi.org/10.1093/hmg/ddq529

539 Chitnis, A.B., 1995. The role of Notch in lateral inhibition and cell fate specification. Mol
540 Cell Neurosci 6, 311–321.

541 Collier, J.R., Monk, N.A., Maini, P.K., Lewis, J.H., 1996. Pattern formation by lateral
542 inhibition with feedback: a mathematical model of delta-notch intercellular
543 signalling. J Theor Biol 183, 429–446. https://doi.org/10.1006/jtbi.1996.0233

544 Dagogo-Jack, I., Shaw, A.T., 2018. Tumour heterogeneity and resistance to cancer
545 therapies. Nat Rev Clin Oncol 15, 81–94.
546 https://doi.org/10.1038/nrclinonc.2017.166

547 Dunwoodie, S.L., Henrique, D., Harrison, S.M., Beddington, R.S., 1997. Mouse Dll3: a
548 novel divergent Delta gene which may complement the function of other Delta
549 homologues during early pattern formation in the mouse embryo. Development
550 124, 3065–3076. https://doi.org/10.1242/dev.124.16.3065

551 Formosa-Jordan, P., and D. Sprinzak. 2014. 'Modeling Notch signaling: a practical
552 tutorial', *Methods Mol Biol*, 1187: 285-310.

553 Gay, C.M., Stewart, C.A., Park, E.M., Diao, L., Groves, S.M., Heeke, S., Nabet, B.Y.,
554 Fujimoto, J., Solis, L.M., Lu, W., Xi, Y., Cardnell, R.J., Wang, Q., Fabbri, G., Cargill,
555 K.R., Vokes, N.I., Ramkumar, K., Zhang, B., Della Corte, C.M., Robson, P.,
556 Swisher, S.G., Roth, J.A., Glisson, B.S., Shames, D.S., Wistuba, I.I., Wang, J.,
557 Quaranta, V., Minna, J., Heymach, J.V., Byers, L.A., 2021. Patterns of transcription
558 factor programs and immune pathway activation define four major subtypes of
559 SCLC with distinct therapeutic vulnerabilities. Cancer Cell 39, 346-360.e7.
560 https://doi.org/10.1016/j.ccell.2020.12.014

561 Geffers, I., Serth, K., Chapman, G., Jaekel, R., Schuster-Gossler, K., Cordes, R.,
562 Sparrow, D.B., Kremmer, E., Dunwoodie, S.L., Klein, T., Gossler, A., 2007.
563 Divergent functions and distinct localization of the Notch ligands DLL1 and DLL3
564 in vivo. The Journal of Cell Biology 178, 465.
565 https://doi.org/10.1083/JCB.200702009

566 Giffin, M.J., Cooke, K., Lobenhofer, E.K., Estrada, J., Zhan, J., Deegen, P., Thomas, M.,
567 Murawsky, C.M., Werner, J., Liu, S., Lee, F., Homann, O., Friedrich, M., Pearson,
568 J.T., Raum, T., Yang, Y., Caenepeel, S., Stevens, J., Beltran, P.J., Canon, J.,
569 Coxon, A., Bailis, J.M., Hughes, P.E., 2021. AMG 757, a half-life extended, DLL3-
570 targeted bispecific T-cell engager, shows high potency and sensitivity in preclinical
571 models of small-cell lung cancer. Clinical Cancer Research 27, 1526–1537.
572 https://doi.org/10.1158/1078-0432.CCR-20-2845

573 Hipp, S., Voynov, V., Drobits-Handl, B., Giragossian, C., Trapani, F., Nixon, A.E., Scheer,
574 J.M., Adam, P.J., 2020. A Bispecific DLL3/CD3 IgG-Like T-Cell Engaging Antibody
575 Induces Antitumor Responses in Small Cell Lung Cancer. Clin Cancer Res 26,
576 5258–5268. https://doi.org/10.1158/1078-0432.CCR-20-0926

577 Hong, D., Knelson, E.H., Li, Y., Durmaz, Y.T., Gao, W., Walton, E., Vajdi, A., Thai, T.,
578 Sticco-Ivins, M., Sabet, A.H., Jones, K., Schinzel, A.C., Bronson, R.T., Nguyen,
579 Q.D., Tolstorukov, M.Y., Vivero, M., Signoretti, S., Barbie, D.A., Oser, M.G.,
580 Plasticity in the Absence of NOTCH Uncovers a RUNX2-Dependent Pathway in

Small cell Lung Cancer. Cancer Res 82(2), 248-263. https://doi.org/10.1158/0008-5472.CAN-21-1991

Ireland, A.S., Micinski, A.M., Kastner, D.W., Guo, B., Wait, S.J., Spainhower, K.B., Conley, C.C., Chen, O.S., Guthrie, M.R., Soltero, D., Qiao, Y., Huang, X., Tarapcsák, S., Devarakonda, S., Chalishazar, M.D., Gertz, J., Moser, J.C., Marth, G., Puri, S., Witt, B.L., Spike, B.T., Oliver, T.G., 2020. MYC Drives Temporal Evolution of Small Cell Lung Cancer Subtypes by Reprogramming Neuroendocrine Fate. Cancer cell. https://doi.org/10.1016/j.ccell.2020.05.001

Jahchan, N.S., Lim, J.S., Bola, B., Peifer, M., 2016. Identification and Targeting of Long-Term Tumor- Propagating Cells in Small Cell Lung Cancer. https://doi.org/10.1016/j.celrep.2016.06.021

Jamal-Hanjani, M., Quezada, S.A., Larkin, J., Swanton, C., 2015. Translational implications of tumor heterogeneity. Clin Cancer Res 21, 1258–1266. https://doi.org/10.1158/1078-0432.CCR-14-1429

Johnson, M.L., Zvirbule, Z., Laktionov, K., Helland, A., Cho, B.C., Gutierrez, V., Colinet, B., Lena, H., Wolf, M., Gottfried, M., Okamoto, I., van der Leest, C., Rich, P., Hung, J.-Y., Appenzeller, C., Sun, Z., Maag, D., Luo, Y., Nickner, C., Vajikova, A., Komarnitsky, P., Bar, J., 2021. Rovalpituzumab Tesirine as a Maintenance Therapy After First-Line Platinum-Based Chemotherapy in Patients With Extensive-Stage-SCLC: Results From the Phase 3 MERU Study. J Thorac Oncol 16, 1570–1581. https://doi.org/10.1016/j.jtho.2021.03.012

Kusumi, K., Sun, E.S., Kerrebrock, A.W., Bronson, R.T., Chi, D.C., Bulotsky, M.S., Spencer, J.B., Birren, B.W., Frankel, W.N., Lander, E.S., 1998. The mouse pudgy mutation disrupts Delta homologue Dll3 and initiation of early somite boundaries. Nature genetics 19, 274–278. https://doi.org/10.1038/961

Ladi, E., Nichols, J.T., Ge, W., Miyamoto, A., Yao, C., Yang, L.T., Boulter, J., Sun, Y.E., Kintner, C., Weinmaster, G., 2005. The divergent DSL ligand Dll3 does not activate Notch signaling but cell autonomously attenuates signaling induced by other DSL ligands. Journal of Cell Biology 170, 983–992. https://doi.org/10.1083/jcb.200503113

Lakes, A.L., An, D.D., Gauny, S.S., Ansoborlo, C., Liang, B.H., Rees, J.A., McKnight, K.D., Karsunky, H., Abergel, R.J., 2020. Evaluating 225Ac and 177Lu Radioimmunoconjugates against Antibody-Drug Conjugates for Small-Cell Lung Cancer. Mol Pharm 17, 4270–4279. https://doi.org/10.1021/acs.molpharmaceut.0c00703

Lim, J.S., Ibaseta, A., Fischer, M.M., Cancilla, B., O'Young, G., Cristea, S., Luca, V.C., Yang, D., Jahchan, N.S., Hamard, C., Antoine, M., Wislez, M., Kong, C., Cain, J., Liu, Y.-W., Kapoun, A.M., Garcia, K.C., Hoey, T., Murriel, C.L., Sage, J., 2017. Intratumoural heterogeneity generated by Notch signalling promotes small-cell lung cancer. Nature 545, 360–364. https://doi.org/10.1038/nature22323

Lim, K.J., Brandt, W.D., Heth, J.A., Muraszko, K.M., Fan, X., Bar, E.E., Eberhart, C.G., 2015. Lateral inhibition of Notch signaling in neoplastic cells. Oncotarget 6, 1666–1677. https://doi.org/10.18632/oncotarget.2762

Malhotra, J., Nikolinakos, P., Leal, T., Lehman, J., Morgensztern, D., Patel, J.D., Wrangle, J.M., Curigliano, G., Greillier, L., Johnson, M.L., Ready, N., Robinet, G., Lally, S.,

Maag, D., Valenzuela, R., Blot, V., Besse, B., 2021. A Phase 1-2 Study of Rovalpituzumab Tesirine in Combination With Nivolumab Plus or Minus Ipilimumab in Patients With Previously Treated Extensive-Stage SCLC. J Thorac Oncol 16, 1559–1569. https://doi.org/10.1016/j.jtho.2021.02.022

Nelson, B.R., Hartman, B.H., Ray, C.A., Hayashi, T., Bermingham-McDonogh, O., Reh, T.A., 2009. Acheate-scute like 1 (Ascl1) is required for normal delta-like (Dll) gene expression and notch signaling during retinal development. Dev Dyn 238, 2163–2178. https://doi.org/10.1002/dvdy.21848

Ohsawa, R., Kageyama, R., 2008. Regulation of retinal cell fate specification by multiple transcription factors. Brain Res 1192, 90–98. https://doi.org/10.1016/j.brainres.2007.04.014

Peltomaa, R., Barderas, R., Benito-Peña, E., Moreno-Bondi, M.C., 2022. Recombinant antibodies and their use for food immunoanalysis. Anal Bioanal Chem 414, 193–217. https://doi.org/10.1007/s00216-021-03619-7

Raum, T., Blümel, C., Dahlhoff, C., Hoffmann, P., Kufer, P., Lutterbüse, R., Nahrwold, E., Pendzialek, J., 2017. Antibody constructs for dll3 and cd3. US20170037130A1.

Rudin, C.M., Brambilla, E., Faivre-Finn, C., Sage, J., 2021. Small-cell lung cancer. Nature Reviews Disease Primers 7, 1–20. https://doi.org/10.1038/s41572-020-00235-0

Rudin, C.M., Poirier, J.T., Byers, L.A., Dive, C., Dowlati, A., George, J., Heymach, J.V., Johnson, J.E., Lehman, J.M., MacPherson, D., Massion, P.P., Minna, J.D., Oliver, T.G., Quaranta, V., Sage, J., Thomas, R.K., Vakoc, C.R., Gazdar, A.F., 2019. Molecular subtypes of small cell lung cancer: a synthesis of human and mouse model data. Nat Rev Cancer 19, 289–297. https://doi.org/10.1038/s41568-019-0133-9

Saunders, L.R., Bankovich, A.J., Anderson, W.C., Aujay, M.A., Bheddah, S., Black, K.A., Desai, R., Escarpe, P.A., Hampl, J., Laysang, A., Liu, D., Lopez-Molina, J., Milton, M., Park, A., Pysz, M.A., Shao, H., Slingerland, B., Torgov, M., Williams, S.A., Foord, O., Howard, P., Jassem, J., Badzio, A., Czapiewski, P., Harpole, D.H., Dowlati, A., Massion, P.P., Travis, W.D., Pietanza, M.C., Poirier, J.T., Rudin, C.M., Stull, R.A., Dylla, S.J., 2015. A DLL3-targeted antibody-drug conjugate eradicates high-grade pulmonary neuroendocrine tumor-initiating cells in vivo. Science Translational Medicine 7. https://doi.org/10.1126/scitranslmed.aac9459

Schaffer, B.E., Park, K.S., Yiu, G., Conklin, J.F., Lin, C., Burkhart, D.L., Karnezis, A.N., Sweet-Cordero, E.A., Sage, J., 2010. Loss of p130 accelerates tumor development in a mouse model for human small-cell lung carcinoma. Cancer Research 70, 3877–3883. https://doi.org/10.1158/0008-5472.CAN-09-4228

Serth, K., Schuster-Gossler, K., Kremmer, E., Hansen, B., Marohn-Köhn, B., Gossler, A., 2015. O-fucosylation of DLL3 is required for its function during somitogenesis. PLoS One 10, e0123776. https://doi.org/10.1371/journal.pone.0123776

Sharma, S.K., Pourat, J., Abdel-Atti, D., Carlin, S.D., Piersigilli, A., Bankovich, A.J., Gardner, E.E., Hamdy, O., Isse, K., Bheddah, S., Sandoval, J., Cunanan, K.M., Johansen, E.B., Allaj, V., Sisodiya, V., Liu, D., Zeglis, B.M., Rudin, C.M., Dylla, S.J., Poirier, J.T., Lewis, J.S., 2017. Noninvasive interrogation of DLL3 expression in metastatic small cell lung cancer. Cancer Research 77, 3931–3941. https://doi.org/10.1158/0008-5472.CAN-17-0299

671 Shue, Y.T., Drainas, A.P., Li, N.Y., Pearsall, S.M., Morgan, D., Sinnott-Armstrong, N.,
672 Hipkins, S.Q., Coles, G.L., Lim, J.S., Oro, A.E., Simpson, K.L., Dive, C., Sage, J.,
673 2022. A conserved YAP/Notch/REST network controls the neuroendocrine cell
674 fate in the lungs. Nat Commun 13, 1–18. https://doi.org/10.1038/s41467-022-
675 30416-2

676 Sjöqvist, M., Andersson, E.R., 2019. Do as I say, Not(ch) as I do: Lateral control of cell
677 fate. Dev Biol 447, 58–70. https://doi.org/10.1016/j.ydbio.2017.09.032

678 Sprinzak, D., Lakhanpal, A., LeBon, L. *et al. Cis*-interactions between Notch and Delta
679 generate mutually exclusive signalling states. *Nature* **465**, 86–90 (2010).
680 https://doi.org/10.1038/nature08959

681 Sprinzak, D., Lakhanpal, A., LeBon, L., Garcia-Ojalvo, J. Elowitz, M.B., 2011. Mutual
682 inactivation of Notch receptors and ligands facilitates developmental patterning.
683 PLoS Comput Biol 7(6): e1002069. https://doi.org/10.1371/journal.pcbi.1002069

684 Stewart, C.A., Gay, C.M., Xi, Y., Sivajothi, S., Sivakamasundari, V., Fujimoto, J., Bolisetty,
685 M., Hartsfield, P.M., Balasubramaniyan, V., Chalishazar, M.D., Moran, C., Kalhor,
686 N., Stewart, J., Tran, H., Swisher, S.G., Roth, J.A., Zhang, J., de Groot, J., Glisson,
687 B., Oliver, T.G., Heymach, J.V., Wistuba, I., Robson, P., Wang, J., Byers, L.A.,
688 2020. Single-cell analyses reveal increased intratumoral heterogeneity after the
689 onset of therapy resistance in small-cell lung cancer. Nat Cancer 1, 423–436.
690 https://doi.org/10.1038/s43018-019-0020-z

691 Sutherland, K.D., Ireland, A.S., Oliver, T.G., 2022. Killing SCLC: insights into how to
692 target a shapeshifting tumor. Genes Dev 36, 241–258.
693 https://doi.org/10.1101/gad.349359.122

694 Tammela, T., Sage, J., 2020. Investigating Tumor Heterogeneity in Mouse Models. Annu
695 Rev Cancer Biol 4, 99–119. https://doi.org/10.1146/annurev-cancerbio-030419-
696 033413

697 Torab, P., Yan, Y., Ahmed, M., Yamashita, H., Warrick, J.I., Raman, J.D., DeGraff, D.J.,
698 Wong, P.K., 2021. Intratumoral Heterogeneity Promotes Collective Cancer
699 Invasion through NOTCH1 Variation. Cells 10, 3084.
700 https://doi.org/10.3390/cells10113084

701 Tully, K.M., Tendler, S., Carter, L.M., Sharma, S.K., Samuels, Z.V., Mandleywala, K.,
702 Korsen, J.A., Delos Reyes, A.M., Piersigilli, A., Travis, W.D., Sen, T., Pillarsetty,
703 N., Poirier, J.T., Rudin, C.M., Lewis, J.S., 2022. Radioimmunotherapy Targeting
704 Delta-like Ligand 3 in Small Cell Lung Cancer Exhibits Antitumor Efficacy with Low
705 Toxicity. Clinical Cancer Research 28, 1391–1401. https://doi.org/10.1158/1078-
706 0432.ccr-21-1533

707 Wei, W., Rosenkrans, Z.T., Liu, J., Huang, G., Luo, Q.-Y., Cai, W., 2020. ImmunoPET:
708 Concept, Design, and Applications. Chem Rev 120, 3787–3851.
709 https://doi.org/10.1021/acs.chemrev.9b00738

710 Weisser, N.E., Hall, J.C., 2009. Applications of single-chain variable fragment antibodies
711 in therapeutics and diagnostics. Biotechnol Adv 27, 502–520.
712 https://doi.org/10.1016/j.biotechadv.2009.04.004

713 Williamson, S.C., Metcalf, R.L., Trapani, F., Mohan, S., Antonello, J., Abbott, B., Leong,
714 H.S., Chester, C.P.E., Simms, N., Polanski, R., Nonaka, D., Priest, L., Fusi, A.,

Carlsson, F., Carlsson, A., Hendrix, M.J.C., Seftor, R.E.B., Seftor, E.A., Rothwell, D.G., Hughes, A., Hicks, J., Miller, C., Kuhn, P., Brady, G., Simpson, K.L., Blackhall, F.H., Dive, C., 2016. Vasculogenic mimicry in small cell lung cancer. Nature Communications 7, 1–14. https://doi.org/10.1038/ncomms13322

Figures and Figure Legends

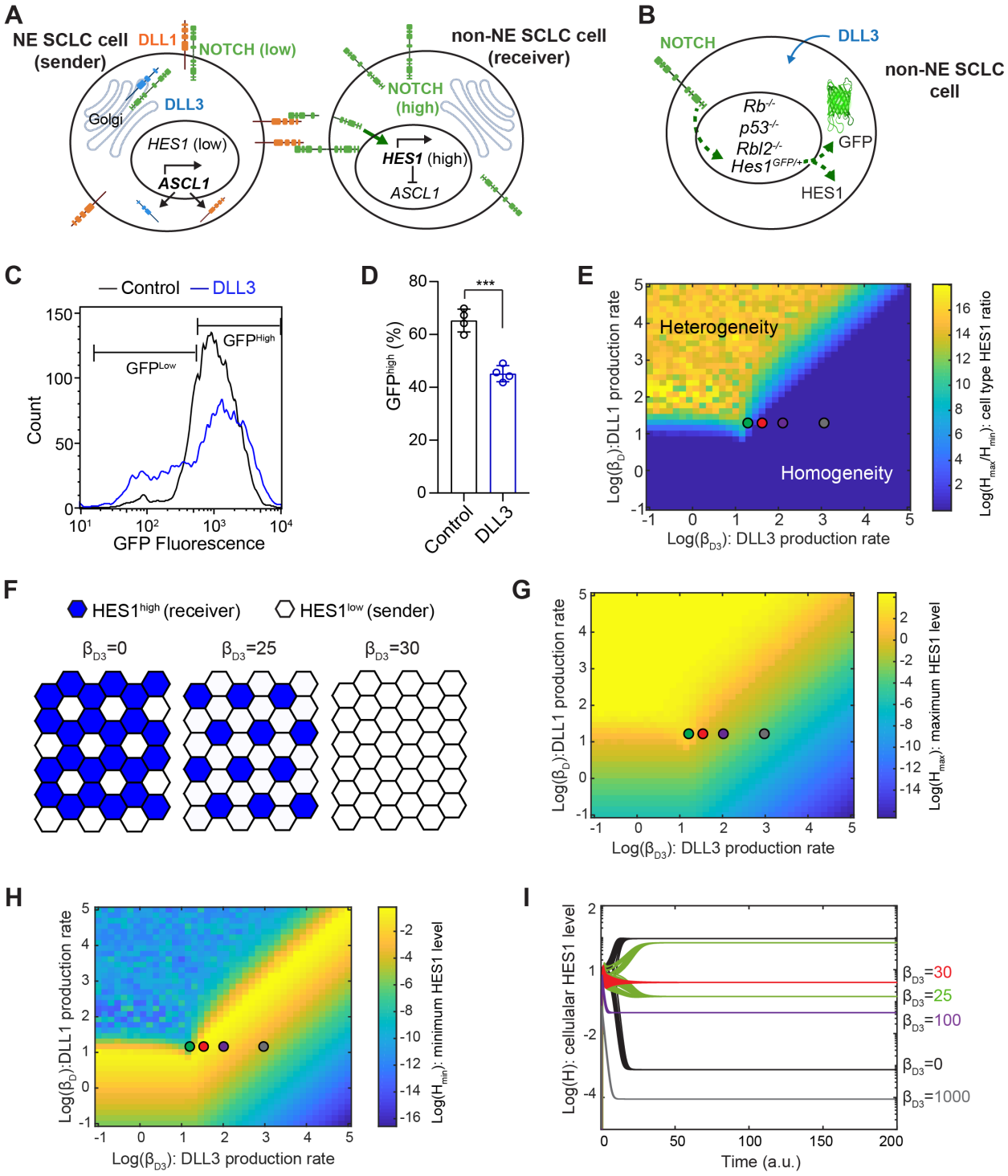

Figure 1. Mathematical model of mutual inactivation shows production rate dependent role of DLL3. (**A**) Schematic of Notch, DLL1, and DLL3 interaction in lateral inhibition with mutual inactivation (LIMI). (**B**) Schematic of HES1^{GFP}-positive cells from an

724 *Rb;p53;Rbl2;Hes1*^{GFP} tumor serving as a reporter cell line, with GFP expression from the
725 *Hes1* locus to monitor the effect of DLL3 expression in regulating Notch activity. (**C**) Flow
726 cytometry of HES1^{GFP}-positive cells with (blue) and without (black) ectopic expression of
727 DLL3 (representative of n = 4 biological replicates). (**D**) Percentage of GFP^{high} HES1^{GFP}-
728 positive cells with and without ectopic expression of DLL3. Unpaired t-test, data
729 represented as mean ± s.d. ***$p<0.001$ (**E**) $\text{Log}(H_{max}/H_{min})$ at steady state were calculated
730 as a function of β_{D3} and β_{D}. Regions with values greater than 0 (light blue to yellow
731 regions) support patterning, while those with 0 (dark blue) do not. (**F**) Hexagonal cell
732 lattice with LIMI showing that DLL3 expression can lead to sparser patterns of higher
733 HES1 cells (blue) or no pattern (homogeneous color). (**G**) H_{max} as a function of β_{D3} and
734 β_{D}. (**H**) H_{min} as a function of β_{D3} and β_{D}. (**I**) Simulations with the indicated parameters for
735 β_{D3} showing H levels in cells with high and low final H levels. Green, red, purple, and gray
736 dots in (E), (G), and (H) correspond to the parameters used in (I).

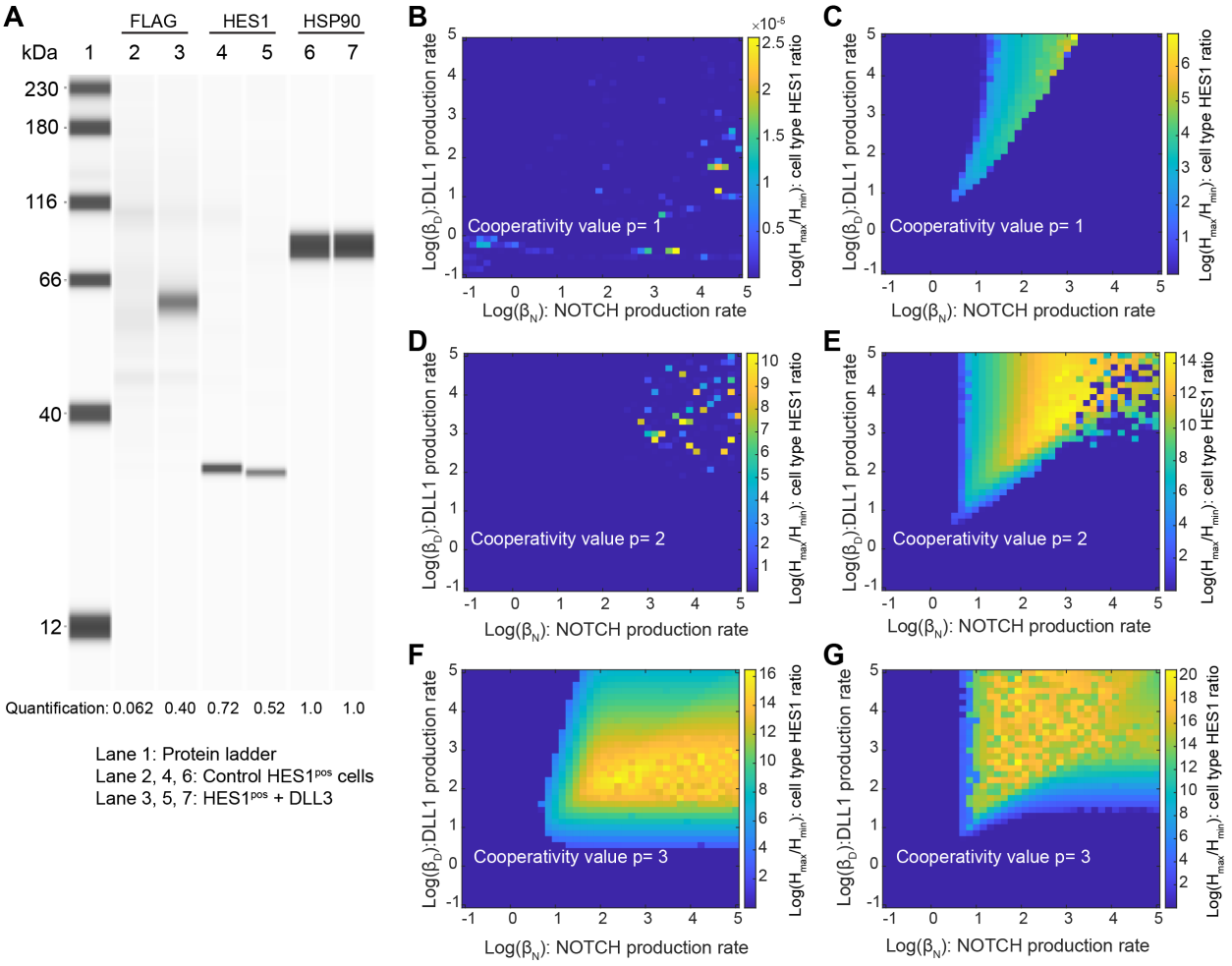

Figure S1 related to Figure 1. Ectopic expression of DLL3 in HES1^{GFP}-positive cells. (**A**) Immunoassay measuring DLL3 and HES1 expression in control HES1^{GFP}-positive cells and the same cells with stable expression of DLL3. HSP90 serves as a loading control. The expected molecular weights of DLL3, HES1, and HSP90 are 65 kDa, 30 kDa, and 90 kDa, respectively. The band intensities were quantified and normalized by those of HSP90. (**B-G**) Log(H_{max}/H_{min}) at steady state were calculated as a function of β_N and β_D without (**B, D, F**) and with (**C, E, G**) mutual inactivation using different values of the feedback loop cooperativity, p. Regions with values greater than 0 (light blue to yellow regions) support patterning, while those with 0 (dark blue) do not. As was shown in the studies by Sprinzak *et al.*, when p = 1 mutual inactivation was required to support patterning in the tested parameter space. Note the different scale in (**B**) (x10^{-5}).

Table S1 related to Figure 1: Parameter values for mathematical modeling

See equations in Methods and Figure 1

Figure	Equations	Parameters	Initial conditions
1E,G,H	1–4	$\gamma = 1$, $k_e = 0.1$, $k_{DR} = 1$, $k_f = 0.1$, $Y_s = 1$, $p = 3$, $k_{RS} = 300000$, $Y_R = 1$, $\beta_N = 20$, $\beta_H = 1000000$, $m = 1$, sigma = 0.1, $k_c = 0.1$, $k_t = 1$, β_D = 0.1 to 1e5, β_{D3} = 0.1 to 1e5	Cells initially set in low values of NOTCH, DLL1, and DLL3 with small variability.
1F	1–4	$\gamma = 1$, $k_e = 0.1$, $k_{DR} = 1$, $k_f = 0.1$, $Y_s = 1$, $p = 3$, $k_{RS} = 300000$, $Y_R = 1$, $\beta_D = 15$, $\beta_N = 20$, $\beta_H = 1000000$, $m = 1$, sigma = 0.1, $k_c = 0.1$, $k_t = 1$, β_{D3} = 0, 25, 30	Cells initially set in low values of NOTCH, DLL1, and DLL3 with small variability.
1I	1–4	$\gamma = 1$, $k_e = 0.1$, $k_{DR} = 1$, $k_f = 0.1$, $Y_s = 1$, $p = 3$, $k_{RS} = 300000$, $Y_R = 1$, $\beta_D = 15$, $\beta_N = 20$, $\beta_H = 1000000$, $m = 1$, sigma = 0.1, $k_c = 0.1$, $k_t = 1$, β_{D3} = 0, 25, 30, 100, 1000	Cells initially set in low values of NOTCH, DLL1, and DLL3 with small variability.
S1B-G	1–4	$\gamma = 1$, $k_e = 0.1$, $k_{DR} = 1$, $k_f = 0.1$, $Y_s = 1$, $p = 3$, $k_{RS} = 300000$, $Y_R = 1$, β_D = 0.1 to 1e5, β_N = 0.1 to 1e5, $\beta_H = 1000000$, $m = 1$, sigma = 0.1, $k_c = 0.1$, $k_t = 1$, $\beta_{D3} = 0$	Cells initially set in low values of NOTCH and DLL1 with small variability.

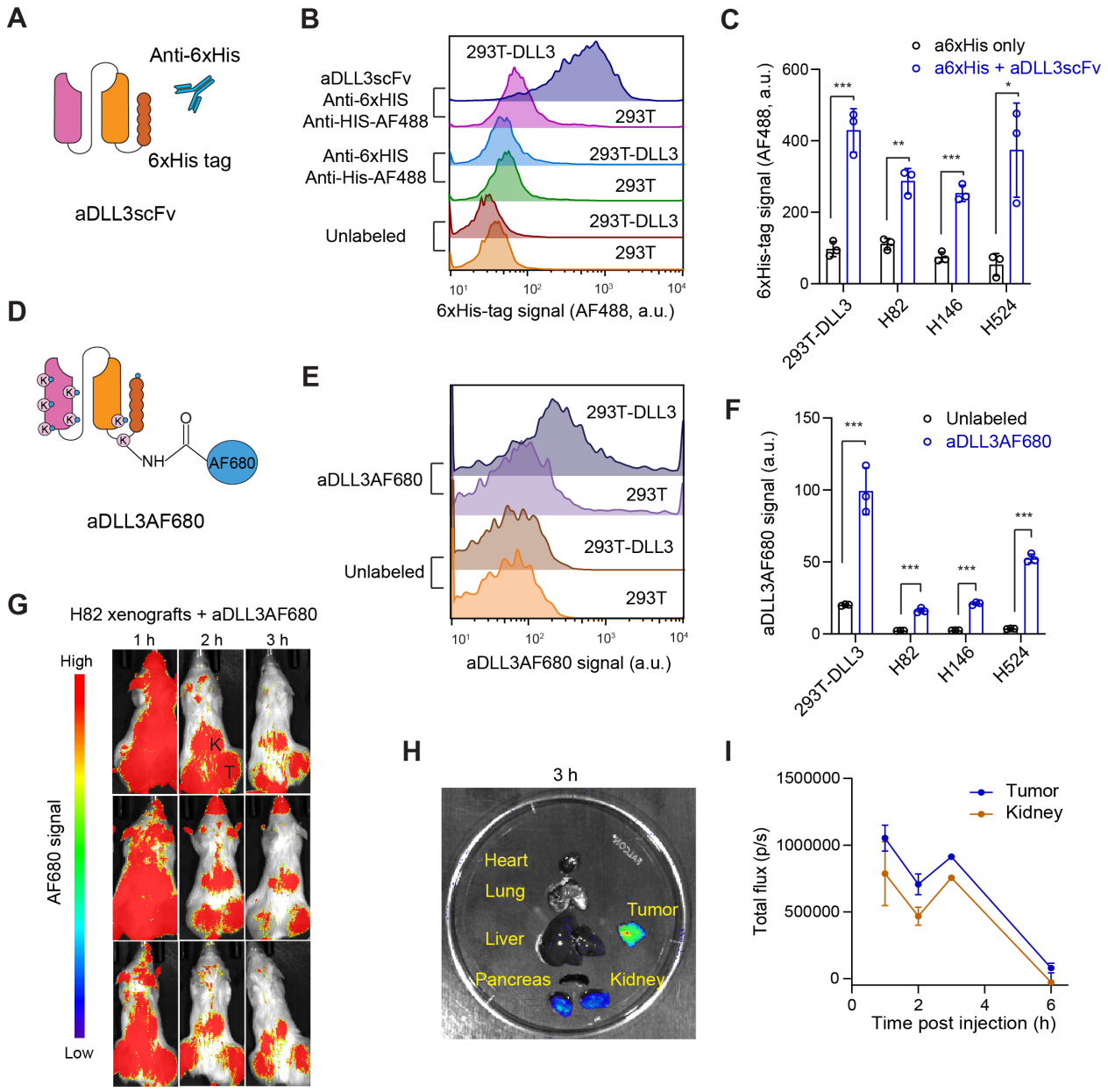

Figure 2. Detection of DLL3 expression at the surface of cells using anti-DLL3 scFv. (**A**) Schematic representation of the His-tagged scFv targeting DLL3 (aDLL3scFv) and the detection of cells expressing DLL3 using this molecule. (**B**) Representative flow cytometry analysis of DLL3 expression in 293T cells expressing exogenous mouse DLL3 using aDLL3scFv (from n=3 biological replicates). (**C**) Quantification of DLL3 detection in 293T-DLL3 cells from (B) and human SCLC cell lines. (**D**) Schematic representation of AF680 labeled aDLL3scFv (aDLL3AF680). (**E**) Representative flow cytometry showing

760 binding activity of aDLL3AF680 (from n=3 biological replicates). (**F**) Quantification of (E)
761 in human SCLC cell lines. (**G**) Whole body fluorescent images of H82 tumor xenografts
762 with 2 nmol of AF680-labeled scFv injected via tail vein. Tumors (T) and kidneys (K) are
763 indicated. (**H**) Representative *ex vivo* imaging of an NCI-H82 bearing mice in (H). (**I**)
764 Quantification of imaging signals, reported as the total flux (p/s) (n=3). Unpaired t-test,
765 data represented as mean ± s.d. $p<0.05$, $^{**}p<0.01$, $^{***}p<0.001$.

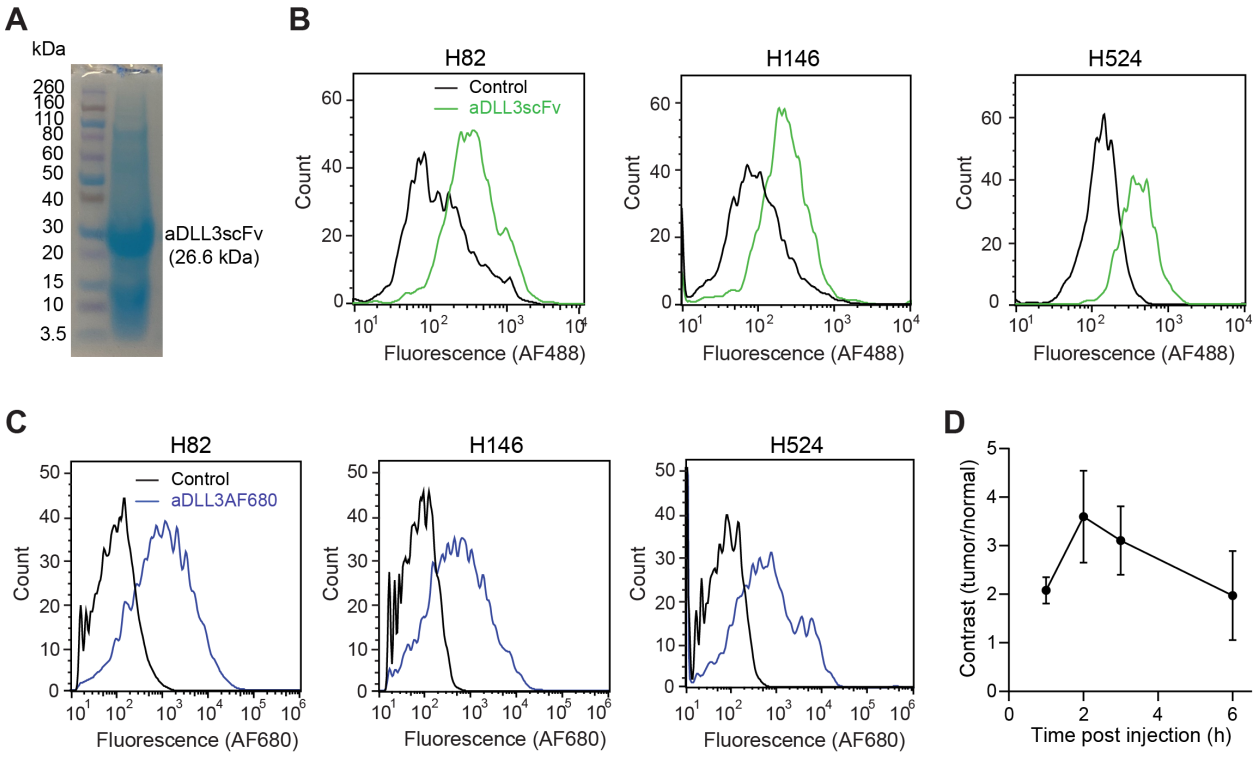

Figure S2 related to Figure 2. Anti-DLL3 scFv binds to human SCLC cells *in vitro* and *in vivo*. (**A**) SDS-PAGE gel stained with SimplyBlue Safe Stain showing aDLL3scFv purified using nickel-NTA affinity column. (**B**) Representative flow cytometry histograms showing binding of human SCLC cells to His-tagged aDLL3scFv, which was detected using rabbit anti-His antibody and AF488 labeled anti-rabbit antibody. (**C**) Representative flow cytometry histograms showing binding of aDLL3AF680 to human SCLC cells. (**D**) Quantification of imaging contrast reported as the ratio of fluorescent signals for tumor versus normal tissue. Error bars represent s.d., n = 3.

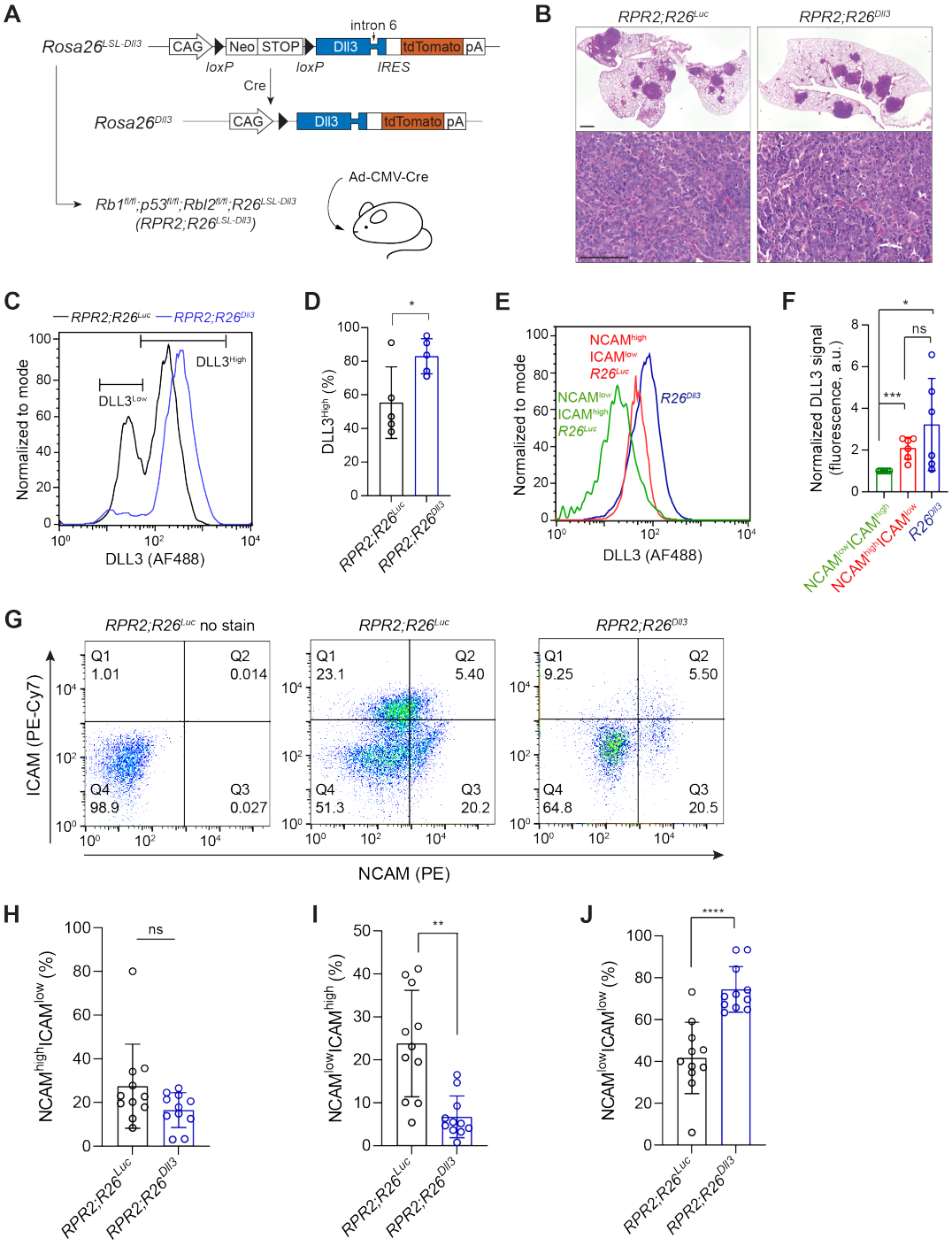

Figure 3. DLL3 expression perturbs the balance between neuroendocrine and non-neuroendocrine cells in a mouse model of SCLC. (**A**) Schematic representation of the Cre-inducible *Dll3* allele and the genetically engineered mouse model of SCLC. (**B**) Representative hematoxylin and eosin (H&E) staining of representative sections from *RPR2;R26*^{Luc} and *RPR2;R26*^{Dll3} mutant lungs (top, scale bar 1mm) and lung tumors

781 (bottom, scale bar 100μm) 6 months after tumor initiation (n ≥ 6 mice). (**C**) Representative
782 flow cytometry analysis of DLL3 cell surface expression in SCLC cells from *RPR2;R26*^{Luc}
783 and *RPR2;R26*^{Dll3} mutant mice 5.5 months after tumor initiation. (**D**) Quantification of (**C**)
784 (n=5 independent experiments). (**E**) As in (C) with *RPR2;R26*^{Luc} SCLC cells differentiated
785 by NCAM and ICAM expression. (**F**) Quantification of (E) (n=6 independent experiments).
786 (**G**) Representative flow cytometry dot plots of control cancer cells from *RPR2;R26*^{Luc}
787 tumors with no stain, stained cells from *RPR2;R26*^{Luc} tumors, and stained cells from
788 *RPR2;R26*^{Dll3} tumors (from left to right). (**H-J**) Quantification of NCAM^{high} ICAM^{low},
789 NCAM^{low} ICAM^{high}, and NCAM^{low} ICAM^{low} populations in (G). Unpaired t-test, data
790 represented as mean ± s.d. $p<0.05$, $^{**}p<0.01$, $^{***}p<0.001$.

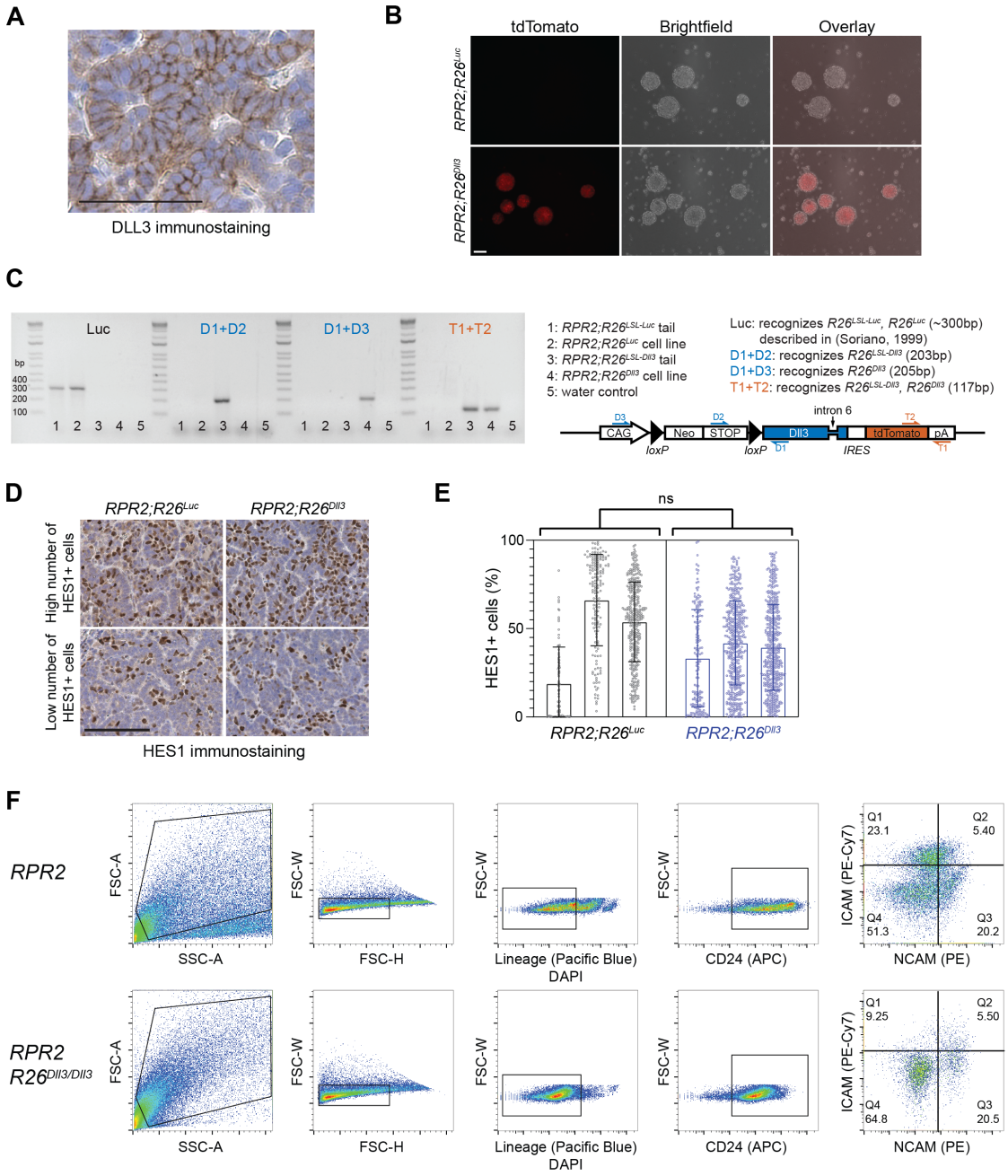

791

792 **Figure S3 related to Figure 3. Characterization of a new mouse allele with inducible**
793 **expression of DLL3.** (**A**) Representative DLL3 immunostaining in an *RPR2;R26^{Luc}*
794 mutant lung tumor section. Scale bar 50μm. (**B**) Representative tdTomato fluorescence
795 and brightfield images of cell lines derived from *RPR2;R26^{Luc}* (top) or *RPR2;R26^{Dll3}*
796 (bottom) mutant lung tumors, scale bar 100μm. (**C**) Genotyping PCR and schematic of

797 allele-specific primer pairs. DNA was extracted from the cell lines shown in (B) and from
798 mouse tails for unrecombined controls. Note that the D1-D3 PCR fragment is too long to
799 be amplified in un-recombined alleles. (**D**) Representative HES1 immunostaining in
800 *RPR2;R26*^{Luc} (left) and *RPR2;R26*^{Dll3} (right) mutant lung tumor sections. Scale bar
801 100μm. (**E**) Quantification of (D). Each point is a 100 μm diameter region within a tumor,
802 and each bar represents a section from an individual mouse. p=0.597 by nested t-test.
803 Error bars represent SD. (**F**) Flow cytometry strategy to analyze NCAM^{high} ICAM^{low} and
804 NCAM^{low} ICAM^{high} SCLC cells from RPR2;R26^{luc} (top) and RPR2;R26^{Dll3} (bottom) mutant
805 mouse SCLC tumors.